International Nano Letters (2020) 10:71–79
https://doi.org/10.1007/s40089-020-00295-w

ORIGINAL ARTICLE

Nano-structured phases of gallium oxide (GaOOH, α-Ga_2O_3, β-Ga_2O_3, γ-Ga_2O_3, δ-Ga_2O_3, and ε-Ga_2O_3): fabrication, structural, and electronic structure investigations

Aditya Sharma[1] · **Mayora Varshney**[2] · **Himani Saraswat**[1] · **Surekha Chaudhary**[1] · **Jai Parkash**[1] · **Hyun-Joon Shin**[3] · **Keun-Hwa Chae**[4] · **Sung-Ok Won**[4]

Received: 18 July 2019 / Accepted: 22 January 2020 / Published online: 4 February 2020

Abstract

Regardless of much curiosity in the synthesis and diversifying properties of the polymorphs of gallium oxide, they are still unrevealed due to their nanoscale size and structural disorders. In this study, convincing methods have been applied to achieve various phases of gallium oxide (i.e., GaOOH, α-Ga_2O_3, β-Ga_2O_3, γ-Ga_2O_3, δ-Ga_2O_3, and ε-Ga_2O_3). X-ray diffraction (XRD) along with Rietveld refinement has been employed to investigate the structural parameters of barely reported phases. Transmission electron microscopy (TEM) images reveal the impact of the protocols of chemical synthesis on the morphology/size of the polymorphs of gallium oxide. Mechanistic discussion on the formation of nano-rod morphology in some of the phases (GaOOH and α-Ga_2O_3) and nano-particle morphology in other (β-Ga_2O_3, γ-Ga_2O_3, δ-Ga_2O_3 and ε-Ga_2O_3) phases is also provided by considering the experimental parameters. The existence of Ga^{3+} ions and their local hybridization with the oxygen is investigated using the X-ray absorption spectroscopy (XAS) at Ga K-edge and conveyed the phase dependence on the hybridization of frontier orbitals.

Keywords XRD · XAS · Polymorphs · Ga_2O_3

Introduction

Gallium oxide is a technologically important semiconductor material and has been utilized in various applications, such as high-temperature gas sensors, semiconducting lasers, field-effect devices, and switching memories [1–5]. Due to its wide band-gap energy (~4.2 eV), this compound has gained much interest for tailoring its electronic and optical properties as an ultraviolet transparent conducting oxide (u-TCO). As a u-TCO, the gallium oxide can extend its applications in solar cells, flat panel display, and phase shift masks for the LASER lithography [6–8]. Its low refractive index (1.8–1.9) also makes it suitable for the single-layered anti-reflecting material for GaAs-based reflecting devices [9]. More recently, nanostructures of gallium oxide have proven themselves suitable materials for the wastewater remediation and combat cancer treatment [10–13].

There are several phases of gallium oxide which have diverse structural, electronic structure, catalytic, and optical properties [14–16]. For example; γ-Ga_2O_3 has exhibited superior catalytic properties over β-Ga_2O_3 phase towards the degradation of water pollutant dyes [17]. The diverse properties in different phases are due to the intriguing occupancy of the Ga^{3+} ions, at the tetrahedral and octahedral sites, and their dissimilar hybridization among the surrounding oxygen ligands.

A few decades ago, interconversions of gallium oxide polymorphs were described by Roy et al. [18]. They applied chemical synthesis for the preparation of compounds. In their work, phase identification was provided in the tabular form based on the powder XRD data. The

---

✉ Aditya Sharma
adityaiuac@gmail.com

[1] Department of Physics, Manav Rachna University, Faridabad, Haryana 121004, India

[2] Department of Applied Physics, School of Vocational and Applied Sciences, Gautam Buddha University, Greater Noida, Uttar Pradesh 201312, India

[3] Pohang Accelerator Laboratory (POSTECH), Pohang, Gyeongbuk 37673, South Korea

[4] Advanced Analysis Centre, Korea Institute of Science and Technology (KIST), Seoul 02792, South Korea

successive literature on the Ga_2O_3 phases is based on the findings of the Roy et al. and the other nano-crystalline phases, such as γ-Ga_2O_3, δ-Ga_2O_3, and ε-Ga_2O_3, were not fully characterized for their structural details and have been hampered by their poor crystalline character [9, 19–21]. In recent years, attempts have been made to fabricate the various phases of gallium oxide with nano-dimensional morphology [22–24]. Less reported phases, i.e., γ-Ga_2O_3, δ-Ga_2O_3, ε-Ga_2O_3, were also examined by applying the pair distribution function (PDF) and neutron diffraction methods [25, 26]. Our group has also synthesized one of the most promising phases of gallium oxide (i.e., γ-Ga_2O_3) using the chemical precipitation method and utilized the X-ray absorption spectroscopy (XAS) technique to examine the effect of Sm doping on its structure, electronic structure, and optical properties [27]. Giving the continuing interest in the structure–property relationship and technological importance to the Ga_2O_3 compounds, we attempted a detailed synthesis, structural, morphology, and electronic structure investigation on the GaOOH, α-Ga_2O_3, β-Ga_2O_3, γ-Ga_2O_3, δ-Ga_2O_3, and ε-Ga_2O_3 phases. Structural parameters of nano-crystalline phases of gallium oxide are obtained using the Rietveld refinements on the XRD patterns. We, mechanistically, discussed the evolution of nano-rod morphology in GaOOH and α-Ga_2O_3 phases and nano-particle morphology in β-Ga_2O_3, γ-Ga_2O_3, δ-Ga_2O_3, and ε-Ga_2O_3 under the light of experimental protocols. Moreover, the distinct electronic structure of various polymorphs of gallium oxide is also studied using the Ga K-edge XAS.

Experimental details

In the first synthesis, 3 g of $Ga(NO_3)_2.xH_2O$ (Gallium nitrate hydrate) was dissolved in 25 ml of deionized water under the magnetic stirring. After achieving a clear solution, the pH was raised up to 11 ± 0.2 by adding liquid ammonia solution and then stirred for 1 more hour. The precipitate was washed several times with the deionized water and dried overnight at 120 °C on the hot plate. The white-colored cake was crushed in mortar–pestle and heated at 500 °C for 6 h. Moreover, a part of the 500 °C annealed sample was also heated at 900 °C for 4 h in the air. In the second synthesis, $Ga(NO_3)_2.xH_2O$ was dissolved into 100 ml ethanol by magnetic stirring. After achieving the clear solution of the precursor, the pH of the solution was raised up 11 ± 0.2 by adding the diluted $H_4N_2.H_2O$ (hydrazine monohydrate) under the magnetic stirring. Abrupt precipitation could be achieved after the involvement of hydrazine monohydrate to the solution. The precipitates were washed several times with ethanol and dried overnight at 120 °C in air. To achieve other polymorphs, the resultant powder was subsequently heated at 500 °C and then 900 °C for 4 h in air. In the third synthesis, the $Ga(NO_3)_2.xH_2O$ was annealed in air at 200 °C for 18 h and white powder was obtained. This white powder sample was heat-treated at 500 °C for 6 h and then at 900 °C for 4 h. The schematic of the different synthesis protocols is presented in Fig. 1.

The structural investigations were performed using the Dmax-2500 (Rigaku) X-ray diffractometer. The X-ray diffraction (XRD) machine was operated at the voltage of 40 kV and a current of 200 mA, and uses a source of Cu Kα

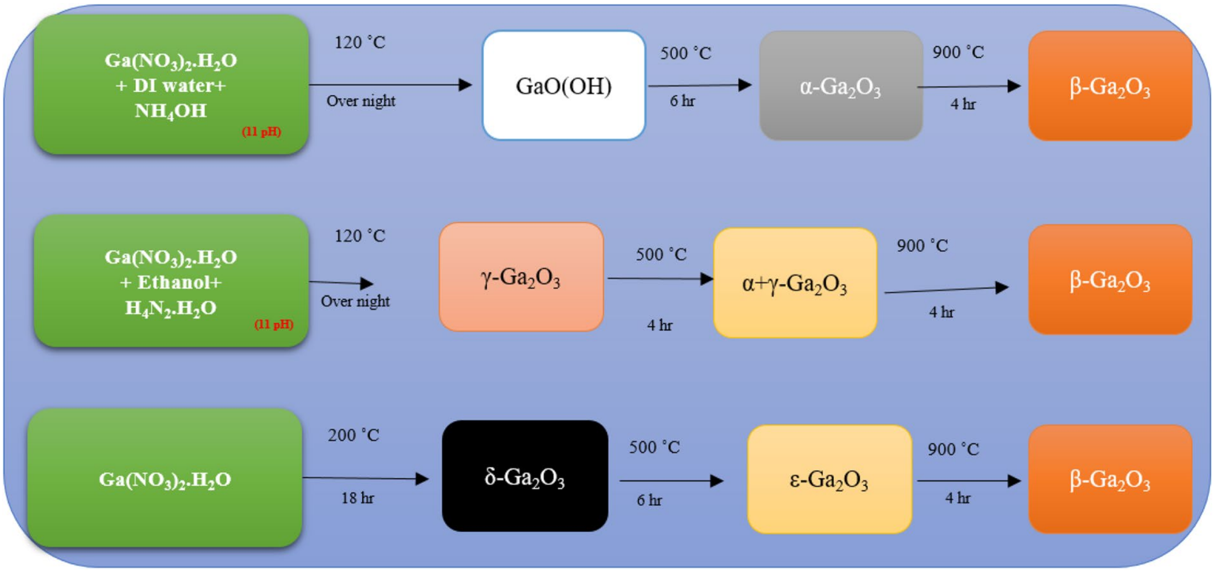

Fig. 1 Schematic of the three different synthesis methods established in this study

radiation ($\lambda = 1.5418$ Å). The scan speed was 1°/min with a step of 0.02°. Transmission electron microscopy (TEM) measurements were performed using the FEI (Talos F200 X) transmission electron microscope. The XAS spectra at Ga K-edge were collected at the 1D XRS (KIST-PAL) beamline of Pohang Accelerator Laboratory (PAL). Sample preparation for XAS, mixture of gasses in the ionization chambers, data collection in transmittance/fluorescence mode, energy calibration, and data normalization for the present experiments were kept similar to our previous experiments on Ga_2O_3:Sm samples [27]. The background removal and normalization of data were done using the ATHENA [28].

Results and discussion

Phase identification and structure details

Figure 2a–c shows the XRD pattern of the samples prepared by the first synthesis method and subsequent heat treatments. The bottom panel shows the XRD patterns of the sample which was prepared by drying the precipitates at 120 °C. XRD patterns show several intense diffraction peaks and are indicating the polycrystalline nature of the samples. All of the diffraction peaks of this sample are matching with the diffraction profile of orthorhombic structured gallium oxyhydroxide (GaOOH) compound (JCPDF #04-010-9861). After the heat treatment (at 500 °C), a new set of diffraction peaks was appeared and did not match with the XRD peaks of gallium oxyhydroxide compound. The XRD patterns of this sample could match with the JCPDF#04-002-2609 file for a rhombohedral structured α-Ga_2O_3 compound. Similar XRD patterns were also observed in the previous reports for the α-Ga_2O_3 [29, 30]. Thus, the XRD results of 120 °C and 500 °C heat-treated samples convey the single-phase formation of GaOOH and α-Ga_2O_3 phases, respectively. Furthermore, annealing at 900 °C temperature leads to a distinct phase formation as evidenced in Fig. 2c. All of the XRD peaks of 900 °C annealed sample were fairly resembled those listed in the JCPDF #04-002-2603 file for a monoclinic structured β-Ga_2O_3 phase and reported in the literature [15–17]. The average crystallite size (D) of these three samples was estimated using the Scherrer relation; $D = 0.9\lambda/\beta\mathrm{Cos}\theta$ (D is the crystallite size, λ is the wavelength of used X-rays, and β is the full width at half maximum of the diffraction peak (three most intense peaks in the XRD patterns were examined and the instrument broadening effect was not included in such calculations). The estimated crystallite size of GaOOH, α-Ga_2O_3, and β-Ga_2O_3 phases is 33.2 nm, 22.1 nm, and 31.5 nm, respectively.

Figure 3a–c shows the XRD patterns of the second synthesis prepared samples. It is noticeable that a few broadened diffraction peaks are presented in Fig. 3a and are indicating less-crystalline nature of the formed compound. XRD patterns of this sample were matching with the cubic structured

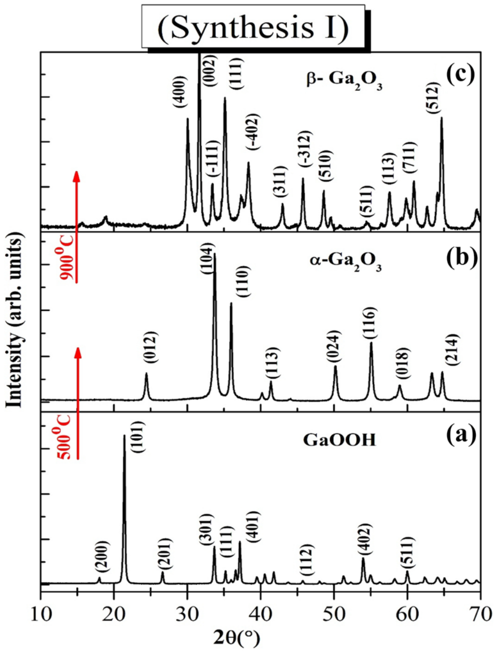

Fig. 2 XRD patterns of first synthesis grown: **a** GaOOH, **b** α-Ga_2O_3, and **c** β-Ga_2O_3 phases

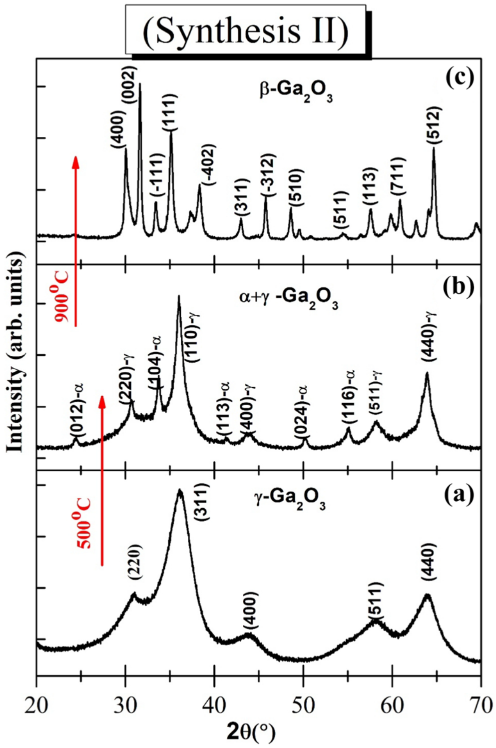

Fig. 3 XRD patterns of second synthesis grown: **a** γ-Ga_2O_3, **b** α-Ga_2O_3 + γ-Ga_2O_3, and **c** β-Ga_2O_3 phases

γ-Ga_2O_3 phase (JCPDF #04-015-6251). Similar XRD patterns of γ-Ga_2O_3 phase were also achieved in our previous study, where the hydrazine monohydrate was employed to prepare the Ga_2O_3:Sm samples [27]. This conveys the reproducibility of the γ-Ga_2O_3 phase by employing our previously established synthesis method. This sample was also heat-treated at 500 °C for 4 h, but only the mixed phases of γ-Ga_2O_3 and α-Ga_2O_3 could be achieved, as shown in Fig. 3b. The symbols (*α*/*γ*) with the (*hkl*) values are representing to the reflections from the *α*/*γ* phases. Heat treatment (at 900 °C) of the mixed-phase sample leads to the formation of single-phase β-Ga_2O_3. Crystallite size of γ-Ga_2O_3 (from Fig. 3a), α-Ga_2O_3 (from Fig. 3b), and β-Ga_2O_3 (from Fig. 3c) phases is 3.3 nm, 18.6 nm, and 30.8 nm, respectively.

Figure 4a–c shows the XRD patterns of the third synthesis prepared samples. The XRD patterns of Fig. 4a are roughly matching with the XRD reflections of δ-Ga_2O_3 phase as reported by Roy et al. [18], Playford et al. [25], and Nishi et al. [31]. However, the broadening of the peaks may not be affirming the single-phase nature of this sample. This compound was further heated at 500 °C and the XRD patterns from the resultant powder sample are displayed in Fig. 4b. There are distinct changes in the XRD peak position and their intensity after the heat treatment of δ-Ga_2O_3 phase. The diffraction peaks of 500 °C heated sample are analogous to the previously reported XRD patterns of ε-Ga_2O_3 phase by Playford et al. (JCPDF #97-023-6278) [26], thus strengthening the ε-Ga_2O_3 phase formation in this study. However, a few of the XRD peaks are not matched either with δ-Ga_2O_3 phase or with ε-Ga_2O_3 phase and suggesting a mixed-phase formation. Detailed quantitative phase analysis is done on δ-Ga_2O_3 and ε-Ga_2O_3 phases, and shall be discussed in the following section. Figure 4c shows the diffraction patterns of the 900 °C annealed sample. All of the diffraction peaks are fairly matching with the monoclinic structured β-Ga_2O_3 phase and in accordance with the previous reports [15–17, 27]. The calculated crystallite sizes for the δ-Ga_2O_3 (from Fig. 4a), ε-Ga_2O_3, (from Fig. 4b), and β-Ga_2O_3 (from Fig. 4c) samples are 6.2 nm, 8.2 nm, and 30.5, respectively.

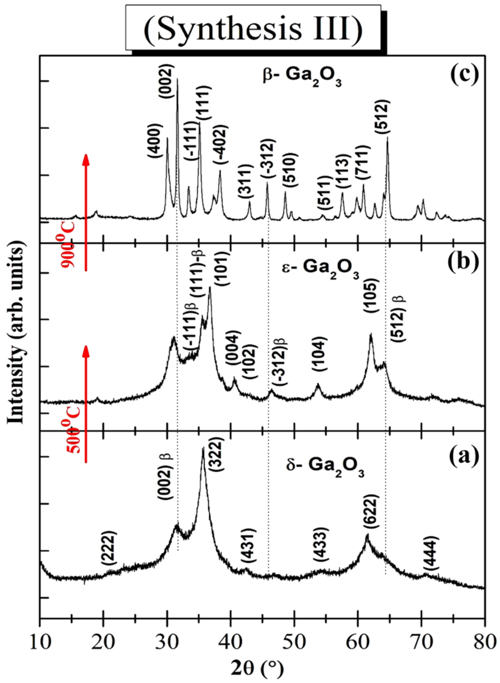

Fig. 4 XRD patterns of third synthesis grown: **a** δ-Ga_2O_3, **b** ε-Ga_2O_3 + β-Ga_2O_3, and **c** β-Ga_2O_3 phases

Figure 5a shows the Rietveld fitted XRD patterns of the GaOOH compound. In the present study, the orthorhombic structure of GaOOH (with a space group of *Pbnm*; $a = 4.516$ Å, $b = 9.779$ Å, and $c = 2.966$ Å) was applied as a starting model. It is noticeable from Fig. 5a that the observed XRD patterns are fairly refined for the starting GaOOH model with a little variation in the lattice parameters [26]. The obtained lattice parameters are tabulated in Table 1. The α-Ga_2O_3 obeys a corundum structure in which the O ions are approximately hexagonal close-packed and Ga^{3+} ions occupy nearly two-thirds of octahedral sites [26]. A rhombohedral crystal structure (space group $R\bar{3}c$) with the lattice parameters of $a = b = 4.9835$ Å and $c = 13.455$ Å was applied to simulate the XRD patterns. It is noticeable from Fig. 5b that the experimentally obtained XRD patterns are properly simulated with the applied structure model. The calculated structural details are also listed in Table 1. The crystal structure of γ-Ga_2O_3 is known as a cation-deficient spinel structure and obeys the partial occupancy of Ga^{3+} ions at, both, octahedral and tetrahedral sites [25–27]. Moreover, the simulated structure of γ-Ga_2O_3 was constructed by choosing the initial structure model of γ-Al_2O_3 [32, 33]. This is because the structural similarity of these two compounds. Moreover, the distribution of Ga^{3+} and Al^{3+} ions, at octahedral and tetrahedral positions, is also similar in their respective compounds. In this study, to simulate the XRD patterns of γ-Ga_2O_3, the ideal spinel structure model was initiated with 16d (octahedral) and 8a (tetrahedral) occupancy of the Ga^{3+} ions. However, this model was not sufficient to simulate the experimental XRD patterns of γ-Ga_2O_3 compounds. Therefore, additional octahedral (8b, 16c) and tetrahedral (48f) sites were added to simulate the XRD results. These two sites are implemented in the model by considering the existence of these two sites in the iso-structural γ-Al_2O_3 phase and also have been anticipated by Playford et al. [25] for simulating the γ-Ga_2O_3 phase. The Rietveld fitted XRD patterns of the nano-crystalline γ-Ga_2O_3 phase are presented in Fig. 5c and the obtained structural parameters are provided in Table 1. The most stable phase of gallium oxide is the β-Ga_2O_3 with monoclinic crystal structure (space group $C_2/_m$) [34, 35]. Under the monoclinic unit cell, the Ga^{3+} ions occupy equal octahedral and tetrahedral sites. To refine the

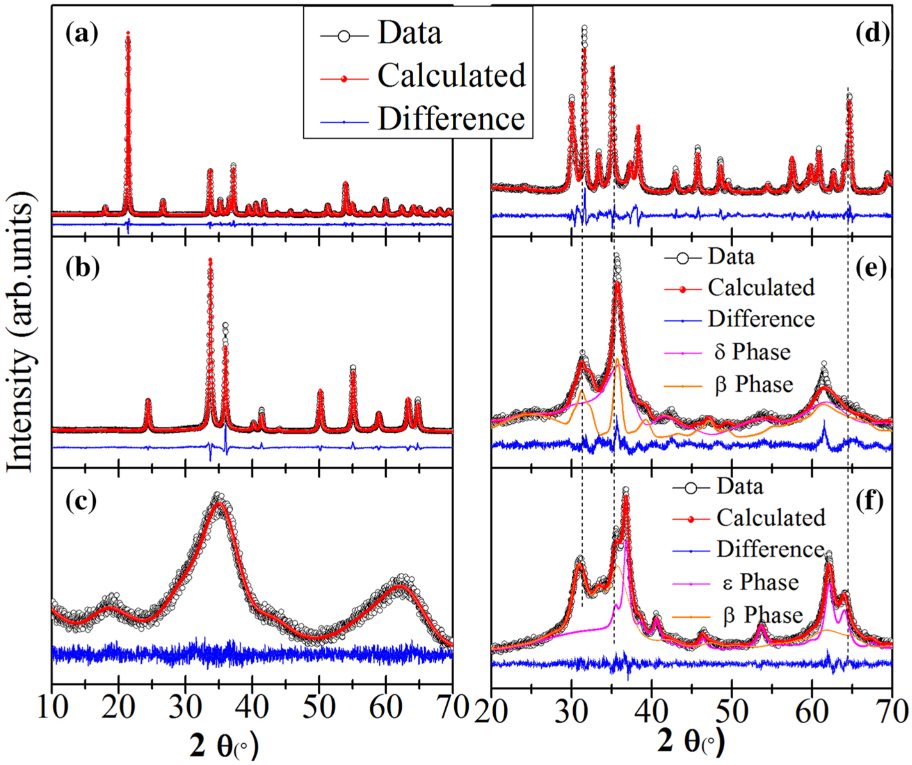

Fig. 5 Rietveld refined XRD patterns of **a** GaOOH, **b** α-Ga_2O_3, **c** γ-Ga_2O_3, **d** β-Ga_2O_3, **e** δ-Ga_2O_3 phase, and **f** ε-Ga_2O_3. Fractional β-Ga_2O_3 phase was integrated to better simulate the XRD patterns of δ-Ga_2O_3 and ε-Ga_2O_3 phases

XRD patterns of β-Ga_2O_3 phase, systematic model with one tetrahedral and one octahedral Ga^{3+} sites was applied as provided in the JCPDF#04-002-2603. Figure 5d shows the Rietveld fitted XRD pattern of β-Ga_2O_3 phase and is convincing the genuineness of the applied structure model. The refined unit cell parameters of β-Ga_2O_3 phase are given in Table 1. The δ-Ga_2O_3 phase was first observed by Roy et al. [18] and was proposed with a bixbyite structure. This structure is also known as *C-type rare earth* and obeys body-centered cubic unit cell with space group of $Ia\bar{3}$. There are several oxide compounds (e.g., In_2O_3, Mn_2O_3, etc.) which also obey the $Ia\bar{3}$ structure with solely octahedral metal sites. We started the Rietveld refinement on the experimental XRD patterns of δ-Ga_2O_3 sample by implementing the model of $Ia\bar{3}$ space group and the lattice parameters of δ-Ga_2O_3 (reported by Roy et al.). However, the fittings for the supposed model were not satisfactory. Therefore, we have applied a quantitative phase analysis on the XRD patterns of δ-Ga_2O_3 phase by assimilating the structural parameters of β-Ga_2O_3 phase. It is clear from Fig. 5e that the spectrum is better simulated when the β-Ga_2O_3 phase is applied in the simulations. Our Rietveld refinement shows that nearly 15% of β-Ga_2O_3 phase is needed to simulate the observed XRD patterns of the δ-Ga_2O_3 phase. In a recent report, it was also considered that the δ-Ga_2O_3 phase is not a distinct phase of gallium oxide, but it is a nano-crystalline modification of ε-Ga_2O_3 phase [26]. This is because of the fact that both local sites of Ga^{3+} ions (i.e., octahedral and tetrahedral) are required to simulate the XRD patterns of the poorly crystalline δ-Ga_2O_3 phase. Thus, we may anticipate that the observed XRD patterns of δ-Ga_2O_3 phase are not originated from the single-phase δ-Ga_2O_3 material, but consist of a partial β-Ga_2O_3 phase, under the nano-crystalline constrain. Similar to the δ-Ga_2O_3 phase, quantitative Rietveld refinement is also employed to simulate the XRD patterns of ε-Ga_2O_3 phase. It is noticeable from Fig. 5f that the XRD spectrum of ε-Ga_2O_3 phase is fairly simulated when ~ 40% of β-Ga_2O_3 phase was integrated with the ε-Ga_2O_3 phase. The Rietveld refinement of XRD pattern of ε-Ga_2O_3 phase conveys that the content of β-Ga_2O_3 phase is increased while compared with the results of δ-Ga_2O_3 phase. This suggests that heat treatment of δ-Ga_2O_3 phase leads to promote β-Ga_2O_3 phase in the compound.

Morphology investigation

Figure 6 shows the TEM images of the first synthesis prepared sample, i.e., (a) GaOOH, (b) α-Ga_2O_3, and (c) β-Ga_2O_3 phases. It is noticeable that the GaOOH sample shows the nano-rod-like morphology with a bit of aggregation. The aggregation is expected in the low-temperature synthesized samples because of the substantial presence of hydroxyl molecules. The nano-rod morphology persists in the case of α-Ga_2O_3 sample which was prepared by heating of GaOOH at 500 °C (see Fig. 6b). The width and length of a typical GaOOH nano-rod sample (the magnified view is presented

Table 1 Structural parameters of the different phases of Ga_2O_3

Sample	Space group	Lattice parameters (Å), Angles (°)	Position of atoms in lattice				Rwp	Goodness of fit
			Site	*x*	*y*	*z*		
GaOOH	Pnma (62)	$a=9.8016(3)$, $b=2.97488(8)$, $c=4.55313(14)$, $\alpha=\beta=\gamma=90$	Ga_1	0.35623(11)	0.25000	0.54721(19)	8.6	1.7
			O_1	0.1949(6)	0.25000	0.2915(11)		
			O_2	0.241(7)	0.75000	0.511(9)		
			H_1	0.4454(6)	0.75000	0.3012(10)		
α-Ga_2O_3	R-3c (176)	$a=b=4.9820(10)$, $c=13.437(3)$, $\alpha=\beta=90$, $\gamma=120$	Ga_1	0.00000	0.00000	0.14440(12)	10.5	1.9
			O_1	0.3073(16)	0.00000	0.25000		
γ-Ga_2O_3	F-d3m (216)	$a=b=c=8.35(15)$, $\alpha=\beta=\gamma=90$	Ga_1	0.00000	0.00000	0.00000	5.1	1.4
			Ga_2	0.75000	0.75000	0.75000		
			Ga_3	0.37115	0.37115	0.37115		
			Ga_4	0.23200	0.00000	0.00000		
			Ga_5	0.97800	0.25000	0.25000		
			O_1	0.13567	0.13567	0.13567		
β-Ga_2O_3	C2/m (12)	$a=12.2169(19)$, $b=3.0392(4)$, $c=5.8095(8)$, $\alpha=\gamma=90$, $\beta=103.811(11)$	Ga_1	0.08249	0.00000	0.32215	10.4	1.4
			O_1	0.15223	0.00000	0.52278		
			O_2	0.20188	0.00000	0.21165		
			Ga_2	0.34215	0.00000	0.19608		
			O_3	0.51348	0.00000	0.11035		
δ-Ga_2O_3 + β-Ga_2O_3 *	Ia-3 (206)	$\mathrm{a}=11.018974(6)$, $\alpha=\beta=\gamma=90$	Ga_1	0.16238	0.00000	0.25000	8.0	1.5
			O_1	0.49215	0.16465	0.57040		
			Ga_2	0.25000	0.25000	0.25000		
ε-Ga_2O_3 + β-Ga_2O_3 *	$P6_3mc$ (186)	$a=\mathrm{b}=2.8936(14)$, $c=9.233(4)$, $\alpha=\beta=90$, $\gamma=120$	Ga_1	0.33333	0.66667	0.33298	6.0	1.3
			Ga_2	0.66667	0.33333	0.83212		
			Ga_2	0.33333	0.66667	0.53052		
			O_1	0.00000	0.00000	1.14445		
			O_2	0.33333	0.66667	0.73252		

The parenthesis values of lattice parameters show errors therein. G.F. is the abbreviation goodness of fittings

*15% and 40% β-Ga_2O_3 phase was incorporated to simulate the δ-Ga_2O_3 and ε-Ga_2O_3 compounds, respectively. In such simulations, the Ga and O sites of β-Ga_2O_3 were implemented as obtained from the pure β-Ga_2O_3 phase

in the inset of Fig. 6a) are 0.2 µm and 1.8 µm, respectively. The length and width of the nano-rods of α-Ga_2O_3 sample are nearly the same as that of GaOOH sample. However, the moisture or hydroxyl molecule-induced aggregation is likely to be eradicated under heat treatment.

In the context of nano-rod formation in aqueous synthesis, it was predicted that the presence of a permanent dipole moment in the starting granules of the compounds (during the aging and growth process) could guide to the oriented attachment of grains into linear chains which led to elongated or rod-like morphology formation [36]. In the case of GaOOH, the oxyhydroxide ligands may form a dipole with the Ga^{3+} ions and the coalescence of such dimers can result in the nano-rod morphology in a similar manner which was observed in the previous report for ZnO nano-rods [37]. Moreover, the nano-rod morphology is persisted under the heat treatment at 500 °C (i.e., in α-Ga_2O_3 sample). In Fig. 6c, larger sized particles of nearly the spherical morphology are seen. The spherical morphology persists minimum surface energy over the other morphologies and the thermal energy-induced spherical grain growth is a common phenomenon in many of the oxide compounds [38]. Therefore, the 900 °C annealed sample has exhibited the distinct morphology of spherical particles.

Though the second synthesis also follows a wet chemical route, the morphology of the product (i.e., γ-Ga_2O_3) is not elongated. Instead of nano-rod formation, we have observed a granular product with low dimensions. The particles seem to be surrounded by an apparent amorphous layer (Fig. 7a). This could be due to the application of ethanol and hydrazine monohydrate solutions in the second synthesis. The ethanol is a polar medium that can help to disperse the granules of the compound and may prevent the elongated morphology. Moreover, partial organic material (amorphous) may exist in the second synthesis (see Fig. 7a). This may come from the spontaneous reaction between hydrazine monohydrate and $Ga(NO_3)_2.xH_2O$ and can persist under the low-temperature (120 °C) drying process. Furthermore, an increase in

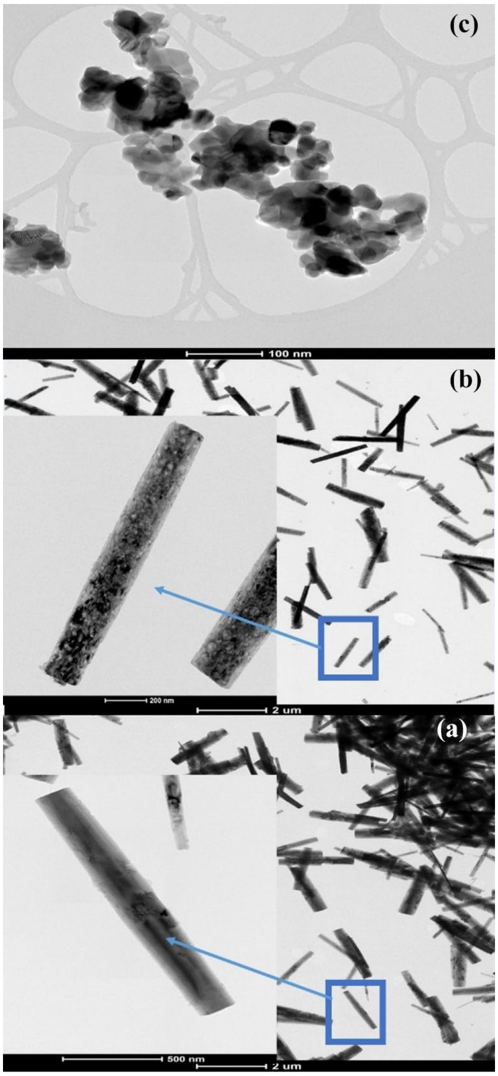

Fig. 6 TEM images of first synthesis prepared samples: **a** GaOOH, **b** α-Ga_2O_3, and **c** (f) β-Ga_2O_3

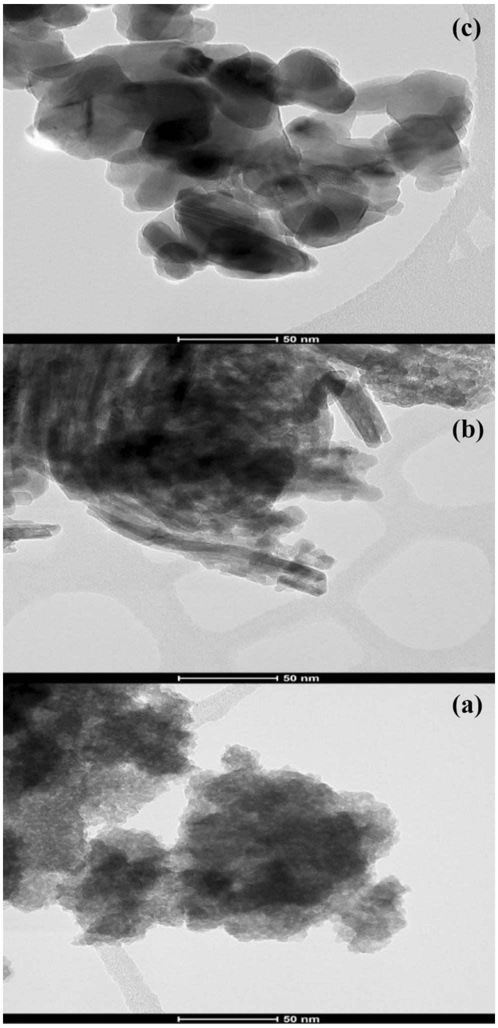

Fig. 7 TEM images of second synthesis prepared samples: **a** γ-Ga_2O_3, **b** γ-Ga_2O_3 $_+$ α-Ga_2O_3, and **c** β-Ga_2O_3

the temperature (500 °C) has manifested the agglomeration/growth of particles into imprecise morphologies. The annealing of the sample at 900 °C leads to diffusion/growth of larger sized particles which is similar to the first synthesis prepared sample.

Small-sized particles and a trace of amorphous material can also be seen in Fig. 8a. This could be due to the remaining organic compound in the 200 °C heated $Ga(NO_3)_2.xH_2O$ and less growth/crystallization process at this temperature. The particles are fairly grown in the 500 °C heated samples and the TEM image shows minimal organic/amorphous component in this sample (see Fig. 8b). Much larger sized and diffused particles (of size ~ 28–38 nm) are seen in Fig. 8c for the β-Ga_2O_3 phase and the organic component also seems to be eliminated at this temperature. The size estimated from TEM image is corresponding to the crystalline size estimated from XRD results, for this sample. The increased particle size in the 900 °C annealed samples could be due to the heat energy-induced growth and diffusion of the small particles into larger sized particles [38].

Electronic structure investigation by XAS

The Ga K-edge X-ray absorption near-edge structure (XANES) spectra originate from the 1 s → 4p transitions and can be used for understanding the local electronic structure differences among the gallium oxide polymorphs [27, 31]. Figure 9 shows the Ga K-edge XANES spectra of different polymorphs of gallium oxide. It is noticeable that the edge-energy position of Ga K-edge spectra of all the polymorphs is nearly identical and conveys the dominancy of Ga^{3+} ions in all of the samples. However, the main white-line peak (between 10,370–10,385 eV) shows spectral intrigues for the different polymorphs. It is evidenced that the white-line

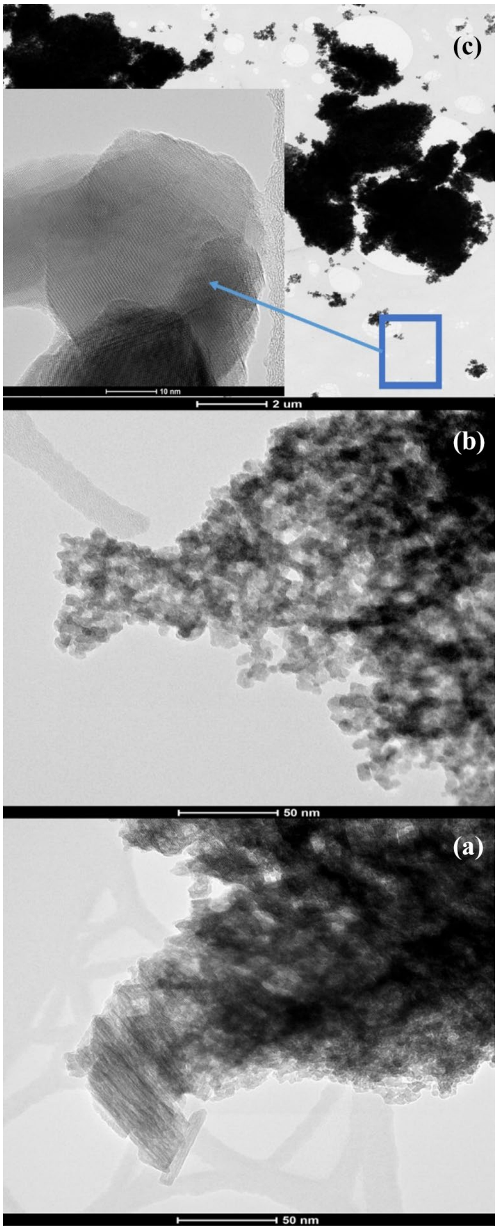

Fig. 8 TEM images of third synthesis prepared samples: **a** δ-Ga_2O_3, **b** ε-Ga_2O_3, and **c** β-Ga_2O_3

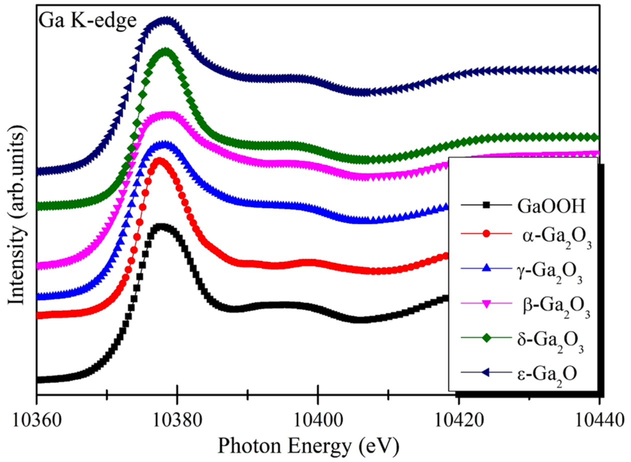

Fig. 9 Ga K-edge XANES spectra of different polymorphs of Ga_2O_3. Two vertical lines represent the two components in the white-line peak

peak shows a broadening in some of the phases, while other polymorphs show a distinct peak. For example; the α-Ga_2O_3 and δ-Ga_2O_3 phases show distinct white-line peaks, while the other phases show broadened white-line feature. In a previous report, closer examination of the Ga K-edge spectra of α-Ga_2O_3 and GaAs was done which conveyed ~ 2 eV energy difference in white-line peak position [39]. The valence state of Ga ions is identical (i.e., Ga^{3+}) in these two compounds (i.e., α-Ga_2O_3 and GaAs). Higher energy white-line peak position of α-Ga_2O_3, compared with GaAs, was attributed to the diverse site occupancy of Ga atoms. The Ga atoms reside in destroyed octahedral sites in α-Ga_2O_3 compound; however, the regular tetrahedral sites are favorable in the GaAs [31, 39]. Therefore, the broadened feature in the white-line peak in some of the polymorphs of Ga_2O_3 can be anticipated as a mixture of tetrahedral and octahedral occupancy of the Ga^{3+} ions. As stated in the XRD results, that α -Ga_2O_3 and δ-Ga_2O_3 phases obey the corundum type and C-type rare-earth structures, respectively, and both of them contain the octahedral sites of Ga atoms. Therefore, the XANES spectra in Fig. 9 show the distinct peak for these two samples. The broadening of white-line peak is much apparent for the γ-Ga_2O_3, β-Ga_2O_3, and ε-Ga_2O_3 phases, and conveys the significant mixture of tetrahedral and octahedral occupancy of the Ga^{3+} ions in such phases. It is in accordance with the previous reports which convey broadened white-line feature and diverse filling of tetrahedral and octahedral sites in γ-Ga_2O_3, β-Ga_2O_3, and ε-Ga_2O_3 phases [31, 40]. In all such phases, the β-Ga_2O_3 contains distinct 50–50% of tetrahedral and octahedral sites, respectively [27, 40, 41]. Moreover, diverse occupancy of tetrahedral and octahedral sites is conceivable in such phases which is subjected to the dopant concentration, crystallite size, and morphology of the compound [25–27, 41].

Conclusions

Three different synthesis methods have been applied for preparing the barely reported phases of gallium oxide. A slight variation in the synthesis solvents could facilitate diverse phase formation and conveyed a strong dependency of the polymorphism on the synthesis methods. Moreover, the size and morphology of the polymorphs were also adjusted with the variation in the synthesis protocols. The presence of permanent dipole moment in the starting granules of the GaO-(OH) complexes has helped to the oriented attachment of grains into linear chains which lead to elongated or rod-like morphology formation in GaOOH and α-$\mathrm{Ga_2O_3}$ phases. Structural parameters were derived for the barely reported phases using the Rietveld refinements. GaOOH, α-$\mathrm{Ga_2O_3}$, and β-$\mathrm{Ga_2O_3}$ phases could be refined properly with the existing structure models, however; the additional octahedral and tetrahedral sites were needed to simulate the XRD patterns of γ-$\mathrm{Ga_2O_3}$ phase. This indicates that the γ-$\mathrm{Ga_2O_3}$ phase does not obey regular cubic structure, but consists of the cation-deficient spinel structure. Much ambiguity is seen in the refinements of δ-$\mathrm{Ga_2O_3}$ and ε-$\mathrm{Ga_2O_3}$ phases. A fractional β-$\mathrm{Ga_2O_3}$ phase was needed; ~ 15% and ~ 40% for simulating the XRD patterns of δ-$\mathrm{Ga_2O_3}$ and ε-$\mathrm{Ga_2O_3}$ phases, respectively. $\mathrm{Ga^{3+}}$ ions are dominantly present in all of the synthesized polymorphs. Dissimilar hybridization of the O 2*p* orbitals and metal 4*s*/4*p* orbitals is clearly seen in the Ga K-edge XANES because of the diverse occupancy of $\mathrm{Ga^{3+}}$ ions at tetrahedral and octahedral sites in different polymorphs of gallium oxide.

Acknowledgements Aditya Sharma is thankful to the Vice-Chancellor and dean of research, Manav Rachna University Faridabad, for providing financial assistance and constant encouragement/support. He is also thankful to Dr. Jitendra Pal Singh (PAL, Pohang, South Korea) for helping in the collection and analysis of XAS data. This work is also partly supported by the Basic Science Research Program (NRF-2015R1A5A1009962) through the National Research Foundation of Korea (NRF) funded by the Korea government.

References

1. Lin, H.J., Gao, H., Gao, P.X.: Appl. Phys. Lett. **110**, 043101 (2017)
2. Pozina, G., Forsberg, M., Kaliteevski, M.A., Hemmingsson, C.: Sci. Rep. **7**, 42132 (2017)
3. Mu, W., Yin, Y., Jia, Z., Wang, L., Sun, J., Wang, M., Tang, C., Hu, Q., Gao, Z., Zhang, J., Lin, N., Veronesi, S., Wang, Z., Zhao, X., Tao, X.: RSC Adv. **7**, 21815 (2017)
4. Kim, J., Mastro, M.A., Tadjer, M.J., Kim, J., Appl, A.C.S.: Mater. Interfaces **10**, 29724 (2018)
5. Wen, X.H., Ming, H.Q., Zhong, J.G., Bing, L.S., Tao, P., Ming, L.: Nano. Res. Lett. **13**, 290 (2018)
6. Chua, D., Kim, S.B., Gordon, R.: AIP Adv. **9**, 055203 (2019)
7. Muhammed, M.M., Roldan, M.A., Yamashita, Y., Sahonta, S.L., Ajia, I.A., Iizuka, K., Kuramata, A., Humphreys, C.J., Roqan, I.S.: Sci. Rep. **6**, 29747 (2016)
8. Shan, F.K., Liu, G.X., Lee, W.J., Lee, G.H., Kim, I.S., Shin, B.C.: J. Appl. Phys. **98**, 023504 (2005)
9. Passlacki, M., Schubert, E.F., Hobson, W.S., Hong, M., Moriya, N., Chu, S., Konstadinidis, K., Mannaerts, J.P., Schnoes, M.L., Zydzik, G.J.: J. Appl. Phys. **77**, 686 (1995)
10. Soto, E.R., Connell, O., Dikengil, F., Peters, P.J., Clapham, P.R., Ostroff, G.R.: J. Drug Deliv. **2016**, 8520629 (2016)
11. Adams, W.T., Ivanisevic, A.: ACS Omega **4**, 6876 (2019)
12. Rodríguez, C.I.M., Álvarez, M.Á.L., Rivera, J.J.F., Arízaga, G.G.C., Michel, C.R.: ECS J. Solid State Sci. Technol. **8**, Q3180 (2019)
13. Li, X., Zhen, X., Meng, S., Xian, J., Shao, Y., Fu, X., Li, D.: Environ. Sci. Technol. **47**, 9911 (2013)
14. Manandhar, S., Ramana, C.V.: Appl. Phys. Lett. **110**, 061902 (2017)
15. Battu, A.K., Manandhar, S., Shutthanandan, V., Ramana, C.V.: Chem. Phys. Lett. **684**, 363 (2017)
16. Pearton, S.J., Yang, J., Cary, P.H., Ren, F., Kim, J., Tadjer, M.J., Mastro, M.A.: Appl. Phys. Rev. **5**, 011301 (2018)
17. Ghodsi, V., Jin, S., Byers, J.C., Pan, Y., Radovanovic, P.V.: J. Phys. Chem. C **121**, 9433 (2017)
18. Roy, R., Hill, V.G., Obson, E.F.: J. Am. Chem. Soc. **74**, 719 (1952)
19. Yoshioka, S., Hayashi, H., Kuwabara, A., Oba, F., Matsunaga, K., Tanaka, I.: J. Phys. Condens. Matter **19**, 346211 (2007)
20. Qian, H.S., Gunawan, P., Zhang, Y.X., Lin, G.F., Zheng, J.W., Xu, R.: Cryst. Growth Des. **8**, 1282 (2008)
21. Mazeina, L., Perkins, F.K., Bermudez, V.M., Arnold, S.P., Prokes, S.M.: Langmuir **26**, 13722 (2010)
22. Teng, Y., Song, L.X., Ponchel, A., Yang, Z.K., Xia, J.: Adv. Mater. **26**, 6238 (2014)
23. Zhang, X., Zhang, Z., Huang, H., Wang, Y., Tong, N., Lin, J., Liu, D., Wang, X.: Nanoscale **10**, 21509 (2018)
24. Gopal, R., Goyal, A., Saini, A., Nagar, M., Sharma, N., Gupta, D.K., Dhayal, V.: Ceram. Int. **44**, 19099 (2018)
25. Playford, H.Y., Hannon, A.C., Barney, E.R., Walton, R.I.: Chem. Eur. J. **19**, 2803 (2013)
26. Playford, H.Y., Hannon, A.C., Tucker, M.G., Dawson, D.M., Ashbrook, S.E., Kastiban, R.J., Sloan, J., Wolton, R.I.: J. Phys. Chem. C **118**, 16188 (2014)
27. Sharma, A., Varshney, M., Shin, H.J., Chae, K.H., Won, S.O.: RSC Adv. **7**, 52543 (2017)
28. Ravel, B., Newville, M.: J. Synchrotron Radiat. **12**, 537 (2005)
29. Quan, Y., Fang, D., Zhang, X., Liu, S., Huang, K.: Mat. Chem. Phys. **121**, 142 (2010)
30. Chen, Y., Xia, X., Liang, H., Abbas, Q., Liu, Y., Du, G.: Cryst. Growth Des. **18**, 1147 (2018)
31. Nishi, K., Shimizu, K.I., Tanamatsu, M., Yoshida, H., Satsuma, A., Tanaka, T., Yoshida, S., Hattori, T.: J. Phys. Chem. B **102**, 10190 (1998)
32. Samain, L., Jaworski, A., Edén, M., Ladd, D.M., Seo, D.K., Garcia, F.J.G., Häussermann, U.: J. Sol. Stat. Chem. **217**, 1 (2014)
33. Paglia, G., Bozin, E.S., Billinge, S.J.L.: Chem. Mater. **18**, 3242 (2006)
34. Roehrens, D., Brendt, J., Samuelis, D., Martin, M.: J. Sol. Stat. Chem. **183**, 532 (2010)
35. Zinkevich, M., Aldinger, F.: J. Am. Ceram. Soc. **87**, 683 (2004)
36. Ethayaraja, M., Bandyopadhyaya, R.: Langmuir **23**, 6418 (2007)
37. Vaghayenegar, M., Kermanpur, A., Abbasi, M.H.: Sc. Iran. F **18**, 1647 (2011)
38. Viana, B.C., Gonçalves, J.S., dos Santos, V., de Santos, M.R., Longo, E., Santos, F.E.P., de Matos, J.M.E.: J. Braz. Chem. Soc. **24**, 1057 (2013)
39. Criado, G.M., Ruiz, J.S., Chu, M.H., Tucoulou, R., López, I., Nogales, E., Mendez, B., Piqueras, J.: Nano Lett. **14**, 5479 (2014)
40. Shimizu, K.I., Tanamatsu, M., Nishi, K., Yoshida, H., Satsuma, A., Tanaka, T., Yoshida, S., Hattori, T.: J. Phys. Chem. B **103**, 1542 (1999)
41. Ghose, S., Rahman, MdS: J. Vac. Sci. Technol. B **34**, 02L109 (2016)